NANO LETTERS

pubs.acs.org/NanoLett Letter

Copper Selenophosphate, Cu_3PSe_4, Nanoparticle Synthesis: Octadecane Is the Key to a Simplified, Atom-Economical Reaction

Nathan A. Neisius, Luke T. MacHale, Erin R. Snyder, Richard G. Finke, and Amy L. Prieto*

Cite This: *Nano Lett.* 2023, 23, 11430−11437 Read Online

ACCESS | Metrics & More | Article Recommendations | Supporting Information

ABSTRACT: Nanoparticle syntheses are designed to produce the desired product in high yield but traditionally neglect atom-economy. Here we report that the simple, but significant, change of the solvent from 1-octadecene (1-ODE) to the operationally inert octadecane (ODA) permits an atom-economical synthesis of copper selenophosphate (Cu_3PSe_4) nanoparticles. This change eliminates the competing selenium (Se) delivery pathways from our first report that required an excess of Se. Instead Se^0_{powder} is dispersed in ODA, which promotes a formal eight-electron transfer between $Cu_{3-x}P$ and Se^0. Powder X-ray diffraction and transmission electron microscopy confirm the purity of the Cu_3PSe_4, while ^1H and ^{13}C NMR indicate the absence of oxidized ODA or Se species. We utilize the direct pathway to gain insights into stoichiometry and ligand identity using thermogravimetric analysis and X-ray photoelectron spectroscopy. Given the prevalence of 1-ODE in nanoparticle synthesis, this approach could be applied to other chalcogenide reaction pathways to improve stoichiometry and atom-economy.

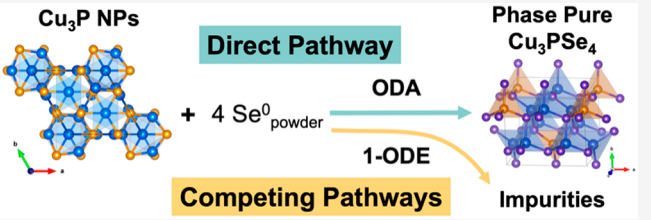

KEYWORDS: *1-octadecene, octadecane, atom-economical, nanoparticle reaction pathway, copper selenophosphate*

Ternary chalcogenide nanoparticles (NPs) have recently gained considerable interest owing to their promising properties for technologically relevant applications, such as photovoltaics,[1−3] thermoelectrics,[4−6] and cathode materials.[7−9] Of particular interest is copper selenophosphate, Cu_3PSe_4, with its theoretical photovoltaic efficiency of 24% and earth abundant elemental composition.[2,10] Historical strategies targeting Cu_3PSe_4 classically involve high temperature solid-state synthetic schemes from traditional elemental precursors (Table S1).[1,7,10−16] A more recent solution-based synthesis of Cu_3PSe_4 NPs from Lee et al. achieved selenization of presynthesized Cu_3P NPs[17] in a one-pot heating method, using a 0.1 M Se^0 powder (Se^0_{powder}) and 1-octadecene (1-ODE) solution.[18] Their approach provided a promising tunable synthesis and potentially low-temperature device processing. However, as noted in our initial report,[18] the 0.1 M Se^0 and 1-octadecene (Se/1-ODE) solution needed to produce Cu_3PSe_4 involves a two-fold excess of Se^0, leading to poor atom-economy and hindering characterization of the several Se species participating in the reaction, *vide infra*.

The use of Se/1-ODE has achieved considerable interest in the colloidal nanoparticle field as a "non-coordinating solvent"[19,20] that eliminates harsh phosphorus reagents to incorporate Se^{2-} in select binary and ternary systems.[21−25] In other systems, existing investigations demonstrate that reactions with Se^0_{powder} and 1-ODE produce Se species of varying reactivity, notably, H_2Se,[26] R_2Se_2,[27−29] and R_2Se.[30] These species introduce multiple reactions, ultimately leading to side reactions and loss of synthetic control of Se-reagent formation.[24] Additionally, the terminal double bond, alpha olefin, of 1-ODE readily polymerizes above 120 °C, which can also effect synthetic control and characterization of intermediates and products.[19,31−35]

Alternatively, primary amines have been employed as a replacement for 1-ODE in NP syntheses,[36−41] where depending on the synthesis, the amines can be the solvent,[42−48] a reagent (reducing agent),[24,48−50] and/or a coordinating ligand.[49,51−54] However, for Cu_3PSe_4 NP syntheses, the substitution of 1-ODE with oleylamine[18] or hexadecylamine (Figure S1) produces Cu−Se binary particles, indicating the importance of Se speciation generated in a Se/1-ODE solution for Cu_3PSe_4 NP formation. Thus, the synthesis of Cu_3PSe_4 NPs with Se/1-ODE can yield undesired byproducts—in the existing synthesis[18] ∼2/3 of Se^0_{powder} is going to products other than the desired Cu_3PSe_4, as a result of multiple, uncontrolled Se species reacting with the metastable,[55] presynthesized Cu_3P NPs (see the Supporting Information for synthetic conditions and reproducibility notes, Figure S2). This reaction, therefore,

Received: July 12, 2023
Revised: November 15, 2023
Accepted: November 16, 2023
Published: December 12, 2023

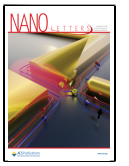

requires a 2-fold excess of Se^0 and produces undesired byproducts, Scheme 1.

Scheme 1. Balanced Reaction Pathways of Cu_3PSe_4 NPs with 1-ODE (A) and ODA (B). Hexadecylamine, HDA, is Shown as the Capping Ligand.[a]

A. *Non-Stoichiometric, competing Se delivery pathway with 1-ODE.*[18]

$1/m(Cu_{3-x}P{\bullet}HDA_n)_m + 12\ Se^0 + a\ 1\text{-ODE (solvent)} \longrightarrow$

$1/p(Cu_{3-x}PSe_4{\bullet}HDA_r)_p + 8\ Se$ by-products [e.g., b H_2Se +

c R_2Se_2 + d R_2Se] + e 2-ODE + f $(1\text{-ODE})_n$ polymer

B. Stoichiometric, atom-economical direct pathway with ODA.

$$1/m(Cu_{3-x}P{\bullet}HDA_n)_m + 4\ Se^0 \xrightarrow{ODA} 1/p(Cu_3PSe_4{\bullet}HDA_r)_p$$

[a]Variables n and r correspond to the ligand coverage of HDA, while m and p represent the number of monomer units.

Despite the nonstoichiometric excess of Se^0_{powder} in our initial reaction,[18] the powder X-ray diffraction (PXRD) pattern of Cu_3PSe_4 under the conditions of Scheme 1A reveals phase purity and the absence of crystalline Se^0 (Figure S3A).[18] However, ^1H NMR confirms the expected presence of excess Se species (Se/1-ODE) and isomerized 1-ODE (Figure S3B).[19,23] It follows that a stoichiometric, atom-economical synthesis of Cu_3PSe_4 is not yet in hand, and competing pathways leading to solution byproducts plague the existing synthesis. Additionally, the lack of a balanced stoichiometry for the current synthesis inhibits one from obtaining important information on the reaction pathway such as determining the variables laid out in Scheme 1A. Hence, developing a more rational, balanced reaction is vital to minimize competing pathways[56] and designing minimalistic, disproof-based[57−59] mechanistic hypotheses[41,60] that, in turn, can inform other, analogous ternary phase syntheses.

Herein, we report that replacing the solvent 1-ODE with octadecane (ODA) is a simple but highly effective method to prepare Cu_3PSe_4 in the form of $(Cu_3PSe_4{\cdot}HDA_r)_p$ NPs via a close-to-stoichiometric, atom-economical synthesis (Scheme 1B). We find that employing ODA promotes a more direct pathway with a net eight-electron transfer at phosphorus, from formally P^{3-} in Cu_3P to formally P^{5+} in Cu_3PSe_4, neatly coupled to the reduction of 4 Se^0 (powder) to 4 Se^{2-} within Cu_3PSe_4. Additionally, to better establish a stoichiometric synthesis, "Cu_3P" is defined and used herein as the Cu deficient, $Cu_{3-x}P$ ($0.133 < x < 1.08$),[61−64] as it has been reported in the literature. We also report preliminary data indicating what amount of HDA is associated with both the starting precursor $(Cu_{3-x}P{\cdot}HDA_n)_m$ and the resultant Se-containing $(Cu_3PSe_4{\cdot}HDA_r)_p$. Finally, the average particle size is determined for both $Cu_{3-x}P$ and Cu_3PSe_4 via TEM to be 102 (± 21.7) and 32 (± 7.8) nm along the long axis, respectively.

As an initial control, the literature-based expectation that Se^{2-} would *not* be incorporated if 1-ODE was replaced with ODA was tested, given the importance of allylic C−H oxidation of the terminal alkene in 1-ODE. *However*, the use of ODA and excess Se^0_{powder} *did* result in the formation of Cu_3PSe_4 ($Pmn2_1$, orthorhombic). Importantly, crystalline Se^0 (Se^0_{cryst}, trigonal) was observed as a side product indicating minimal reaction with ODA (Figure S4). Given that Se is still incorporated even in ODA, we hypothesized that the use of ODA in place of 1-ODE would allow the stoichiometric delivery of Se to form pure Cu_3PSe_4 without Se/1-ODE byproducts, resulting in a better overall atom economy.

Indeed, Cu_3PSe_4 NPs were synthesized using the stoichiometrically required 4 mol equiv of Se^0_{powder} in ODA for 20 min (Scheme 1B). Figure 1A shows the Rietveld refinements (details in Table S2),[65] indicating that 97 wt % of the product indexes to Cu_3PSe_4 with a slight excess of Se^0_{cryst} (3 wt %) excluding any ligand content, *vide infra*. The supernatant was characterized by ^1H, ^{13}C NMR, gas chromatography−mass spectroscopy (GC-MS), and Fourier-transform infrared spectroscopy (FT-IR, Figures 1B, S5−S7, respectively), which displays no deviation from pure ODA and the absence of oxidized byproducts. The downfield shift of 0.88 and 1.26 ppm represents the terminal methyl group (6H, 1.00) and methylene hydrogen environments (32H, 5.35) respectively. Additionally, the supernatant was spiked with 1 mol % of 1-

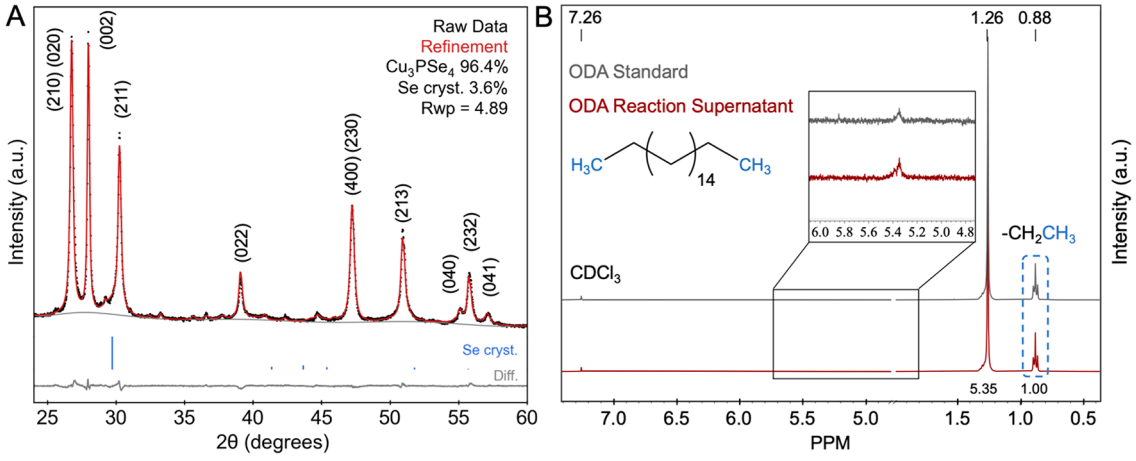

Figure 1. Characterization of the stoichiometric reaction with octadecane as the solvent. (A) Powder X-ray diffraction pattern and Rietveld refinement method of $(Cu_3PSe_4{\cdot}HDA_r)_p$ nanoparticles. Se PDF #00-042-2425 (details in SI) is included to identify the pattern that helps fit the asymmetric peak at 30 2θ. (B) ^1H NMR of the reaction supernatant and pure octadecane, with an inset at 5000× intensity from 4.8 to 6.0 ppm.

https://doi.org/10.1021/acs.nanolett.3c02620
Nano Lett. 2023, 23, 11430−11437

ODE, an expected byproduct if ODA does react with Se^0_{powder}, and that 1% 1-ODE proved detectable by ^1H NMR (Figure S8); however, no detectable (i.e., <1 mol %) 1-ODE is present in the supernatant, in turn implying no (i.e., <1%) H_2Se is formed, nor hence involved, in the improved reaction (i.e., and to the extent (undetected) midchain, internal olefins are not formed). We do detect very low concentrations of midchain alkenes in reactions *containing excess selenium*, but only there presumably as a result of H_2Se generation *after* Cu_3PSe_4 formation, *vide infra* (Figure S9). When the excess selenium is reduced to stoichiometric equivalents, the presence of midchain alkenes is reduced to a negligible amount (Figure S9). Of note, upon quenching the reaction, the extracted supernatant developed a light red tint over an extended time that is hypothesized to be a slight excess of Se,[66−74] where temperature studies confirm the presence of amorphous selenium (a-Se, Figure S10).[67,75] Further details are provided in SI for the interested reader. In short, the use of ODA as a solvent enables a direct reaction pathway with stoichiometric delivery of Se as defined in the balanced reaction in Scheme 1B.

As a control, we returned to 1-ODE, but now using just the four equiv of Se^0_{powder}, to test if stoichiometric Se^0 will work as well as it did in ODA. However, consistent with the hypothesis of 1-ODE leading to a variety of side products (Scheme 1A), a mixture of phases was detected by PXRD (Figure 2), including

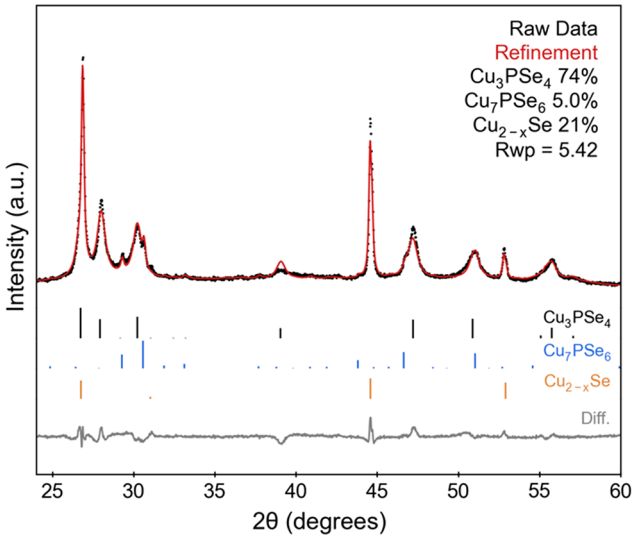

Figure 2. Powder X-ray diffraction pattern for the stoichiometric ratio of Cu_3P + $4Se^0_{powder}$ + 1-ODE with standard synthetic conditions.

$Cu_{2-x}Se$ and Cu_7PSe_6 (refinement details in Table S3). Furthermore, after extending the reaction time to 2 h and overnight, the thermodynamically favored[55] Cu_3PSe_4 is still not the sole phase present, whereas the same time in ODA yields Cu_3PSe_4 as the major product (Figure S11). Given the above results and literature evidence that Se/1-ODE produces species that include H_2Se, R_2Se, and R_2Se_2 (Scheme 1A), the use of ODA is hereby shown to be a simple, effective change to synthesize Cu_3PSe_4 that saves 2/3 of the Se^0 otherwise needed to optimize the Cu_3PSe_4 yield. The use of ODA avoids unnecessary, off-path Se traps that then require a 2-fold excess of Se^0_{powder} to drive formation of Cu_3PSe_4, resulting in an overall poor atom-economical synthesis when using the traditional solvent, 1-ODE.

Further indication of a cleaner, direct reaction pathway is illustrated in the transmission electron microscopy (TEM) images and scanning TEM/energy-dispersive X-ray spectroscopy (STEM/EDS) of $(Cu_3PSe_4{\cdot}HDA_r)_p$ (Figures 3, S12–

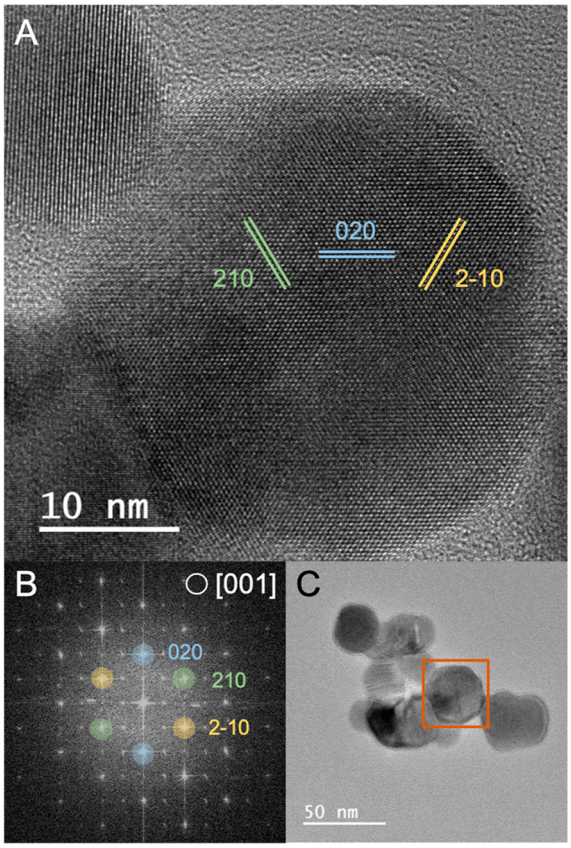

Figure 3. (A) High magnification transmission electron microscopy (TEM), (B) fast Fourier transform (FFT) of particle in (A) and (C) low magnification TEM of $(Cu_3PSe_4{\cdot}HDA_r)_p$ particles under stoichiometric conditions (Scheme 1B).

S14). In our previous publication[18] with Scheme 1A conditions, the resulting Cu_3PSe_4 NPs are noted to have high polydispersity and ill-defined morphology (Figure S15) as a result of indirect, competing reaction pathways. The stoichiometric conditions in Scheme 1B demonstrate that polydispersity is significantly decreased, with size distributions of 24 ± 5.4 and 32 ± 7.8 nm along the short and long axes (Figures 4C and S16), respectively. Additionally, as a result of targeting a more direct reaction pathway, a more crystalline Cu_3PSe_4 product is observed in Figure 3A, with defined lattice planes as compared to the previous synthesis with 1-ODE.[18] The fast Fourier transform (FFT) of Figure 3A produces spots corresponding to the lattice planes with respect to a [001] zone axis (Figure 3B), with *d*-spacings consistent with the orthorhombic crystal structure of Cu_3PSe_4 ($Pmn2_1$). This is further illustrated in Figure S12, where the inverse-fast-Fourier transform (iFFT) of masked FFT spots is overlaid on the corresponding TEM images. Ultimately, the combination of lattice parameters extracted from Rietveld refinement with the structural information from TEM allows us to define Cu_3PSe_4 NPs as $(Cu_3PSe_4{\cdot}HDA_r)_p$, where $p = 2.90\ (\pm 0.04) \times 10^4$ (reference S17 for calculation).

To attain a better understanding of the improved stoichiometry in Scheme 1B, the surface ligand identity and

https://doi.org/10.1021/acs.nanolett.3c02620
Nano Lett. 2023, 23, 11430−11437

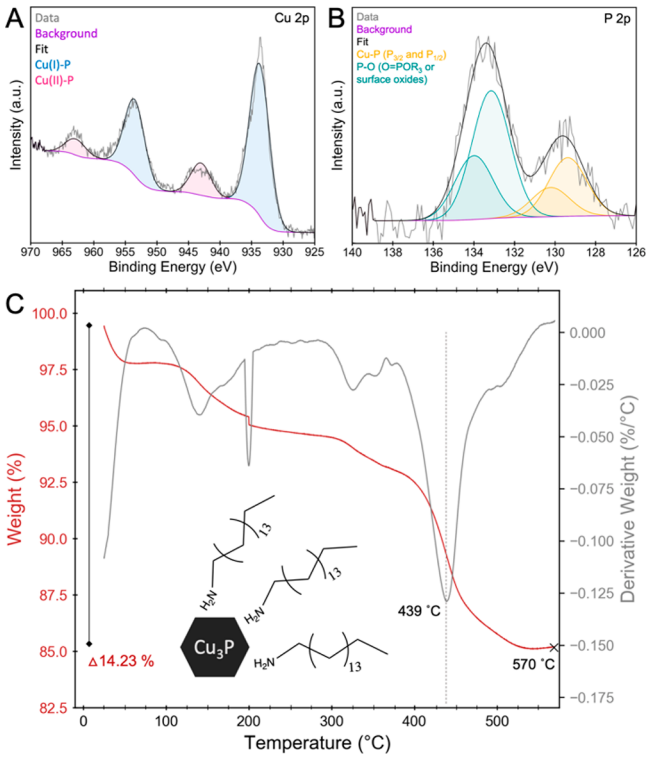

Figure 4. Surface characterization of $Cu_{3-x}P$ particles. (A) XPS of the Cu 2p region and (B) P 2p region. (C) TGA with a 2 °C/min heating profile to 570 °C.

quantity were investigated for both $Cu_{3-x}P$ and Cu_3PSe_4. The surface composition was initially analyzed with ^1H NMR on $Cu_{3-x}P$ particles, washed to remove excess precursors, which was indicative of long alkyl chains consistent with HDA as the primary, surface-bound ligand (Figure S18). Additionally, X-ray photoelectron spectroscopy (XPS) of the carbon (C) and nitrogen (N) 1s regions (Figure S19) is representative of HDA binding environments according to previous literature reports.[54,76,77] Of note, the Cu and P 2p binding region (Figure 4A and B) demonstrates the characteristic $Cu_{3-x}P$ environments,[18,78−83] while the satellite Cu(II) peak (Figure 4B) and P−O peak at 134 eV likely corresponds to surface oxides.[78−80,83] Finally, Cu_3PSe_4 was characterized with XPS for Cu, P, Se, and C bonding environments (Figure S20). The core bonding environments (Cu, P and Se) were consistent with previous reports of Cu_3PSe_4 and Cu_3PS_4,[7−9,84] whereas the C region had similar peaks to $Cu_{3-x}P$ NPs but a decrease in the C-NH_2 environment (Figure S20D). In summary, the spectroscopic evidence mentioned above confirms the sample purity and provides evidence for the nanoparticle surface composition, an important component of the net reaction stoichiometry.

With HDA identified as the surface ligand, the quantity of organic content for $Cu_{3-x}P$ was determined in order to calculate the required Se^0_{powder} molar equivalence in Scheme 1B. First, thermogravimetric analysis (TGA) was performed on dried presynthesized $Cu_{3-x}P$ nanoparticles over a temperature range of 25−570 °C with a 2 °C/min heating profile, resulting in a 14.23% weight loss (Figure 4C) and no degradation of the core particles (Figure S21). Of note, when a 25−800 °C at 10 °C/min heating profile is used (Figure S22A and S23), 2 wt % degradation of $Cu_{3-x}P$ to Cu^0 was quantified with Rietveld refinements (Figures S22B and S24). Of importance to refining the precise stoichiometry, when ∼15 wt % organic content is accounted for in the $Cu_{3-x}P$ mol calculation, the Se content measured via PXRD is reduced from 3.6 to 1.3 wt % in the refined product, $(Cu_3PSe_4{\cdot}HDA_r)_p$ (Figure S25 and S26). The HDA content of the refined product decreased from 15 to 5 wt % (Figure S27), assuming 85 wt % crystalline $Cu_{3-x}P$ as the starting material; however, the $Cu_{3-x}P$ heating profile required to thermally remove the organic content could not be applied to Cu_3PSe_4 due to degradation to Cu_7PSe_6 and P_2Se_5 above 500 °C.[13] The significant decrease in Se content further supports the improved, near-stoichiometric synthesis in Scheme 1B. That said, two aspects of $Cu_{3-x}P$ contributing to the variation in stoichiometry are under a separate investigation and will be described in a future report: (i) the elemental composition and Cu vacancy, *x*, in $Cu_{3-x}P$; and (ii) the effect of the $Cu_{3-x}P$ particle-size dispersion (Figure S28) on the reactivity with Se^0_{powder}.

The results provided herein are consistent with the synthesis of Cu_3PSe_4 as described in Scheme 1B. Overall, an 8 electron (e^-) redox reaction of $(Cu_{3-x}P{\cdot}HDA_n)_m$ with the surface of suspended $(Se^0)_n$ is occurring, especially once the solid selenium becomes molten ca. 221 °C.[66,69,70,85] However, one can raise the question of whether there is any dissolution or other speciation of $(Se^0)_n$ under the 221 °C reaction conditions. Literature studies support the claim of dispersed selenium particles, but moderate solubility has only been observed for select solvents,[45,69,86−88] most notably carbon disulfide,[66,89] hydrazine,[90] and ethylenediamine,[86] but with significantly higher solubility (38 wt % gray selenium) recorded in a binary thiol-amine mixture under ambient conditions.[88] In our own hands, some indirect evidence for a dispersion of Se^0 species is observed in an Se/ODA temperature control (Figure S29), where a color transition is noted only after the melting point to a color distinctly different from the clear solution when $Cu_{3-x}P$ is present. Additionally, the reactivity of Se^0_n with $Cu_{3-x}P$ NPs was monitored by PXRD ex situ studies (Figure S30), which resulted in high conversion to Cu_3PSe_4 at 250 °C and near phase purity at 300 °C.

Even though our demonstration of <1% 1-ODE formation from ODA under our reaction conditions would appear to rule out H_2Se participation in our Cu_3PSe_4 formation reaction (and unless midchain olefins that we do not detect are being formed, vide supra), we decided to further consider and then test the alternative mechanistic hypothesis that $Cu_{3-x}P$ could be reacting at least in part with in situ generated H_2Se to drive ternary phase formation, consistent with previous literature emphasizing H_2Se production in aliphatic hydrocarbon solvents.[21,26,91−93] Recall here that H_2Se has been demonstrated to be a reactive and reasonably efficient selenium precursor for *binary* nanoparticle syntheses, most commonly cadmium selenide (CdSe).[21,26] Moreover, thermodynamic data for *gas-phase* Se_n species formation from crystalline, trigonal $Se^0_{cryst;trig}$ (Table S4) shows that H_2Se (g) formation is the "most favorable" among various possible reactions (Table S4), ΔG^0_{300} = 7.29 kcal mol^{-1}.[94]

However, under similar synthetic conditions used herein, a previous quantitative study revealed that the production of H_2Se from Se^0_{powder} in aliphatic solvents results in only low yield of H_2Se, with gravimetric measurements indicating only 10.5% Se^0 conversion at 320 °C for 1 h in paraffin oil.[92] In addition, the "H_2Se hypothesis" was further tested experimentally in our hands through the direct addition of the

https://doi.org/10.1021/acs.nanolett.3c02620
Nano Lett. 2023, 23, 11430−11437

headspace of an Se/ODA solution (i.e., and hence any H_2Se) to $Cu_{3-x}P$, a control experiment which resulted in *only minor* conversion to the binary product, Cu_2Se (R-3m, trigonal), under otherwise similar synthetic conditions (300 °C, 30 min, Figure S31). In short, the key to the improved stoichiometry described herein is, according to all our evidence: (i) the lack of participation by ODA to form Se-consuming species prior to Cu_3PSe_4 formation, and (ii) a quantitative 8 electron, complimentary redox match between the $Cu_{3-x}P$ reductant and the 4 Se^0 oxidant resulting in 4 Se^{2-} in the Cu_3PSe_4 product—that is, the complementary 8 electron redox half reactions of the formally P^{3-} (Cu_3P) → P^{5+} (Cu_3PSe_4) + 8 e^- and 4 Se^0 + 8 e^- → 4 Se^{2-}.

In conclusion, an improved synthesis of Cu_3PSe_4 has been developed that eliminates Se-containing byproducts that otherwise consume 2/3 of the Se^0 needed to make phase-pure Cu_3PSe_4 in 1-ODE. Simply by replacing 1-ODE with ODA, a much cleaner, close to stoichiometric, near-atom-economical synthesis was obtained, in which 4 Se^0 are reduced by the formally 8 e^- oxidation of P^{3-} in Cu_3P en route to P^{5+} formally present in Cu_3PSe_4, a reaction in which ODA serves predominantly as an inert solvent. Moreover, the results obtained herein form a basis from which more detailed questions regarding the mechanism of formation of Cu_3PSe_4, as well as the synthesis of other ternary phases, most notably Cu_7PSe_6, can be more rationally and directly addressed. Finally, the results presented can also be applied to a myriad of other systems and studies involving 1-ODE, Se^0, and other chalcogenides.

■ ASSOCIATED CONTENT

Supporting Information

The Supporting Information is available free of charge at https://pubs.acs.org/doi/10.1021/acs.nanolett.3c02620.

> Powder X-ray diffraction patterns and corresponding Rietveld refinements, nuclear magnetic resonance spectra, thermogravimetric analysis, Fourier-transform infrared spectroscopy, gas chromatography−mass spectroscopy, transmission electron microscopy, scanning transmission electron microscopy/energy X-ray dispersive spectroscopy, and X-ray photoelectron spectroscopy (PDF)

■ AUTHOR INFORMATION

Corresponding Author

Amy L. Prieto − *Department of Chemistry, Colorado State University, Fort Collins, Colorado 80523, United States;* orcid.org/0000-0001-9235-185X; Email: amy.prieto@colostate.edu

Authors

Nathan A. Neisius − *Department of Chemistry, Colorado State University, Fort Collins, Colorado 80523, United States;* orcid.org/0000-0002-0454-6970

Luke T. MacHale − *Department of Chemistry, Colorado State University, Fort Collins, Colorado 80523, United States;* orcid.org/0000-0002-4148-0771

Erin R. Snyder − *Department of Chemistry, Colorado State University, Fort Collins, Colorado 80523, United States*

Richard G. Finke − *Department of Chemistry, Colorado State University, Fort Collins, Colorado 80523, United States*

Complete contact information is available at: https://pubs.acs.org/10.1021/acs.nanolett.3c02620

Author Contributions

The manuscript was written through contributions of all authors. All authors have given approval to the final version of the manuscript. N.A.N.: data acquisition, conceptualization, analysis, writing; L.T.M.: data acquisition, conceptualization, editing; E.R.S.: data acquisition, analysis, editing; R.G.F.: conceptualization, editing, supervision; A.L.P.: conceptualization, editing, supervision, funding acquisition.

Funding

This work is supported by NSF Macromolecular, Supramolecular, and Nanochemistry (MSN #2109141).

Notes

The authors declare no competing financial interest.

■ ACKNOWLEDGMENTS

The authors wish to thank the Analytical Resources Core (RRID: SCR_021758) at Colorado State University for instrument access, training, and assistance with sample analysis. We also thank Amanda Kale for assistance in electron microscopy.

■ ABBREVIATIONS

Cu_3P, copper phosphide; Cu_3PSe_4, copper selenophosphate; 1-ODE, 1-octadecene; ODA, octadecane; HDA, hexadecylamine; PXRD, powder X-ray diffraction; NMR, nuclear magnetic resonance; FT-IR, Fourier-transform Infrared Spectroscopy; XPS, X-ray photoelectron spectroscopy; TEM, transmission electron microscopy; STEM, scanning transmission electron microscopy; EDS, energy-dispersive X-ray spectroscopy; FFT, fast Fourier transform; iFFT, inverse fast Fourier transform; TGA, thermogravimetric analysis; GC-MS, gas chromatography−mass spectroscopy; Rwp, weighted profile R-factor

■ REFERENCES

(1) Foster, D. H.; Jieratum, V.; Kykyneshi, R.; Keszler, D. A.; Schneider, G. Electronic and Optical Properties of Potential Solar Absorber Cu_3PSe_4. *Appl. Phys. Lett.* **2011**, *99* (18), 181903.

(2) Yu, L.; Kokenyesi, R. S.; Keszler, D. A.; Zunger, A. Inverse Design of High Absorption Thin-Film Photovoltaic Materials. *Adv. Energy Mater.* **2013**, *3* (1), 43−48.

(3) Shi, T.; Yin, W. J.; Al-Jassim, M.; Yan, Y. Structural, Electronic, and Optical Properties of Cu_3-V-VI_4 Compound Semiconductors. *Appl. Phys. Lett.* **2013**, *103* (15), 152105.

(4) Foster, D. H.; Barras, F. L.; Vielma, J. M.; Schneider, G. Defect Physics and Electronic Properties of Cu_3PSe_4 from First Principles. *Phys. Rev. B - Condens. Matter Mater. Phys.* **2013**, *88* (19), 195201.

(5) Slassi, A.; Hammi, M.; El Rhazouani, O.; Arejdal, M. Ab Initio Study of Thermoelectric Properties of Cu_3PSe_4 and Cu_3PS_4: Alternative Materials for Thermoelectric Applications. *Opt. Quantum Electron.* **2017**, *49* (4), 171.

(6) Ma, Z.; Hu, J.; Sa, R.; Li, Q.; Zhang, Y.; Wu, K. Screening Novel Candidates for Mid-IR Nonlinear Optical Materials from I_3-V-VI_4 Compounds. *J. Mater. Chem. C* **2017**, *5* (8), 1963−1972.

(7) Tao, D.; Li, T.; Tang, Y.; Cao, Y.; Xu, F. Copper Tetraselenophosphate Cathode for Rechargeable Magnesium Batteries: A Redox-Active Polyatomic Anion Strategy to Design the Cathode Material. *Chem. Mater.* **2023**, *35* (11), 4525−4531.

(8) Brehm, W.; Santhosha, A. L.; Zhang, Z.; Neumann, C.; Turchanin, A.; Martin, A.; Pinna, N.; Seyring, M.; Rettenmayr, M.; Buchheim, J. R.; Adelhelm, P. Copper Thiophosphate (Cu_3PS_4) as Electrode for Sodium-Ion Batteries with Ether Electrolyte. *Adv. Funct. Mater.* **2020**, *30* (19), No. 1910583.

(9) Tripathy, D.; Sampath, S. Understanding the High Capacity Contributions of Cu_3PS_4 towards Lithium Storage. *J. Power Sources* **2020**, *478*, No. 229066.
(10) Itthibenchapong, V.; Kokenyesi, R. S.; Ritenour, A. J.; Zakharov, L. N.; Boettcher, S. W.; Wager, J. F.; Keszler, D. A. Earth-Abundant Cu-Based Chalcogenide Semiconductors as Photovoltaic Absorbers. *J. Mater. Chem. C* **2013**, *1* (4), 657−662.
(11) Garin, J.; Parthé, E. The Crystal Structure of Cu_3PSe_4 and Other Ternary Normal Tetrahedral Structure Compounds with Composition 1_356_4. *Acta Crystallogr. B* **1972**, *28* (12), 3672−3674.
(12) Ott, R.; Klingen, W.; Hahn, H. Zur Struktur Des Cu_3PSe_4. *Naturwissenschaften* **1972**, *59*, 364.
(13) Schulte-Kellinghaus, M.; Kramer, V. Thermogravimetric Investigation of Some Thioorthophosphates and Thiohypodiphosphates. *Thermochim. Acta* **1978**, *27*, No. 141.
(14) Lathrop, D.; Franke, D.; Maxwell, R.; Tepe, T.; Flesher, R.; Zhang, Z.; Eckert, H. Dipolar ^{31}P NMR Spectroscopy of Crystalline Inorganic Phosphorus Compounds. *Solid State Nucl. Magn. Reson.* **1992**, *1*, 73−83.
(15) Francisco, R.; Eckert, H. Compound Formation and Local Structure in Ternary Metal-Phosphorous-Selenium Systems. *J. Solid State Chem.* **1994**, *112*, 270−276.
(16) Canlas, C. G.; Muthukumaran, R. B.; Kanatzidis, M. G.; Weliky, D. P. Investigation of Longitudinal ^{31}P Relaxation in Metal Selenophosphate Compounds. *Solid State Nucl. Magn. Reson.* **2003**, *24*, 110−122.
(17) Liu, J.; Meyns, M.; Zhang, T.; Arbiol, J.; Cabot, A.; Shavel, A. Triphenyl Phosphite as the Phosphorus Source for the Scalable and Cost-Effective Production of Transition Metal Phosphides. *Chem. Mater.* **2018**, *30* (5), 1799−1807.
(18) Lee, J. M.; Kraynak, L. A.; Prieto, A. L. A Directed Route to Colloidal Nanoparticle Synthesis of the Copper Selenophosphate Cu_3PSe_4. *Angew. Chem., Int. Ed.* **2020**, *59* (8), 3038−3042.
(19) Dhaene, E.; Billet, J.; Bennett, E.; Van Driessche, I.; De Roo, J. The Trouble with ODE: Polymerization during Nanocrystal Synthesis. *Nano Lett.* **2019**, *19* (10), 7411−7417.
(20) Pu, C.; Zhou, J.; Lai, R.; Niu, Y.; Nan, W.; Peng, X. Highly Reactive, Flexible yet Green Se Precursor for Metal Selenide Nanocrystals: Se-Octadecene Suspension (Se-SUS). *Nano Res.* **2013**, *6* (9), 652−670.
(21) Yordanov, G. G.; Yoshimura, H.; Dushkin, C. D. Phosphine-Free Synthesis of Metal Chalcogenide Quantum Dots by Means of in Situ-Generated Hydrogen Chalcogenides. *Colloid Polym. Sci.* **2008**, *286* (6−7), 813−817.
(22) Shen, H.; Wang, H.; Li, X.; Niu, J. Z.; Wang, H.; Chen, X.; Li, L. S. Phosphine-Free Synthesis of High Quality ZnSe, ZnSe/ZnS, and Cu-, Mn-Doped ZnSe Nanocrystals. *Dalton Trans.* **2009**, *47*, 10534−10540.
(23) Bullen, C.; Van Embden, J.; Jasieniak, J.; Cosgriff, J. E.; Mulder, R. J.; Rizzardo, E.; Gu, M.; Raston, C. L. High Activity Phosphine-Free Selenium Precursor Solution for Semiconductor Nanocrystal Growth. *Chem. Mater.* **2010**, *22* (14), 4135−4143.
(24) Hou, B.; Benito-Alifonso, D.; Webster, R.; Cherns, D.; Galan, M. C.; Fermín, D. J. Rapid Phosphine-Free Synthesis of CdSe Quantum Dots: Promoting the Generation of Se Precursors Using a Radical Initiator. *J. Mater. Chem. A* **2014**, *2* (19), 6879−6886.
(25) Yu, W. W.; Peng, X. Formation of High-Quality CdS and Other I -VI Semiconductor Nanocrystals in Noncoordinating Solvents: Tunable Reactivity of Monomers. *Angew Chem Int Ed Engl* **2002**, *13*, 2368−2371.
(26) Deng, Z.; Cao, L.; Tang, F.; Zou, B. A New Route to Zinc-Blende CdSe Nanocrystals: Mechanism and Synthesis. *J. Phys. Chem. B* **2005**, *109* (35), 16671−16675.
(27) Brutchey, R. L. Diorganyl Dichalcogenides as Useful Synthons for Colloidal Semiconductor Nanocrystals. *Acc. Chem. Res.* **2015**, *48* (11), 2918−2926.
(28) Tappan, B. A.; Barim, G.; Kwok, J. C.; Brutchey, R. L. Utilizing Diselenide Precursors toward Rationally Controlled Synthesis of Metastable $CuInSe_2$ Nanocrystals. *Chem. Mater.* **2018**, *30* (16), 5704−5713.
(29) Koziel, A. C.; Goldfarb, R. B.; Endres, E. J.; Macdonald, J. E. Molecular Decomposition Routes of Diaryl Diselenide Precursors in Relation to the Phase Determination of Copper Selenides. *Inorg. Chem.* **2022**, *61*, 14673−14683.
(30) Ho, E. A.; Peng, A. R.; Macdonald, J. E. Alkyl Selenol Reactivity with Common Solvents and Ligands: Influences on Phase Control in Nanocrystal Synthesis. *Nanoscale* **2021**, *14* (1), 76−85.
(31) Jana, N. R.; Chen, Y.; Peng, X. Size- and Shape-Controlled Magnetic (Cr, Mn, Fe, Co, Ni) Oxide Nanocrystals via a Simple and General Approach. *Chem. Mater.* **2004**, *16* (20), 3931−3935.
(32) Srivastava, B. B.; Jana, S.; Karan, N. S.; Paria, S.; Jana, N. R.; Sarma, D. D.; Pradhan, N. Highly Luminescent Mn-Doped ZnS Nanocrystals: Gram-Scale Synthesis. *J. Phys. Chem. Lett.* **2010**, *1* (9), 1454−1458.
(33) Chen, B.; Zhong, H.; Zhang, W.; Tan, Z.; Li, Y.; Yu, C.; Zhai, T.; Bando, Y.; Yang, S.; Zou, B. Highly Emissive and Color-Tunable $CuInS_2$-Based Colloidal Semiconductor Nanocrystals: Off-Stoichiometry Effects and Improved Electroluminescence Performance. *Adv. Funct. Mater.* **2012**, *22* (10), 2081−2088.
(34) Gordon, T. R.; Cargnello, M.; Paik, T.; Mangolini, F.; Weber, R. T.; Fornasiero, P.; Murray, C. B. Nonaqueous Synthesis of TiO_2 Nanocrystals Using TiF_4 to Engineer Morphology, Oxygen Vacancy Concentration, and Photocatalytic Activity. *J. Am. Chem. Soc.* **2012**, *134* (15), 6751−6761.
(35) Hamachi, L. S.; Jen-La Plante, I.; Coryell, A. C.; De Roo, J.; Owen, J. S. Kinetic Control over CdS Nanocrystal Nucleation Using a Library of Thiocarbonates, Thiocarbamates, and Thioureas. *Chem. Mater.* **2017**, *29* (20), 8711−8719.
(36) Wang, D.; Li, Y. Effective Octadecylamine System for Nanocrystal Synthesis. *Inorg. Chem.* **2011**, *50* (11), 5196−5202.
(37) Mourdikoudis, S.; Liz-Marzán, L. M. Oleylamine in Nanoparticle Synthesis. *Chem. Mater.* **2013**, *25* (9), 1465−1476.
(38) Ananthakumar, S.; Ram Kumar, J.; Moorthy Babu, S. Evolution of Non-Phosphine Solvents in Colloidal Synthesis of I-III-VI_2 and I_2-II-IV-VI_4 group Semiconductor Nanomaterials − Current Status. *Mater. Sci. Semicond. Process.* **2017**, *67* (May), 152−174.
(39) Lee, J. M.; Miller, R. C.; Moloney, L. J.; Prieto, A. L. The Development of Strategies for Nanoparticle Synthesis: Considerations for Deepening Understanding of Inherently Complex Systems. *J. Solid State Chem.* **2019**, *273*, 243−286.
(40) Mbewana-Ntshanka, N. G.; Moloto, M. J.; Mubiayi, P. K. Role of the Amine and Phosphine Groups in Oleylamine and Trioctylphosphine in the Synthesis of Copper Chalcogenide Nanoparticles. *Heliyon* **2020**, *6* (11), No. e05130.
(41) De Roo, J. Chemical Considerations for Colloidal Nanocrystal Synthesis. *Chem. Mater.* **2022**, *34* (13), 5766−5779.
(42) Wang, D.; Xie, T.; Peng, Q.; Li, Y. Ag, Ag_2S, and Ag_2Se Nanocrystals: Synthesis, Assembly, and Construction of Mesoporous Structures. *J. Am. Chem. Soc.* **2008**, *130* (12), 4016−4022.
(43) Liu, Y.; Yao, D.; Shen, L.; Zhang, H.; Zhang, X.; Yang, B. Alkylthiol-Enabled Se Powder Dissolution in Oleylamine at Room Temperature for the Phosphine-Free Synthesis of Copper-Based Quaternary Selenide Nanocrystals. *J. Am. Chem. Soc.* **2012**, *134* (17), 7207−7210.
(44) Wang, T.-M.; Gao, B.; Wang, Q.; Zhao, M.; Kang, K.-B.; Xu, Z.-G.; Zhang, H.-L. A Facile Phosphine-Free Method for Synthesizing PbSe Nanocrystals with Strong Optical Limiting Effects. *Chem. - Asian J.* **2013**, *8* (5), 912−918.
(45) Walker, B. C.; Agrawal, R. Contamination-Free Solutions of Selenium in Amines for Nanoparticle Synthesis. *Chem. Commun. Camb. Engl.* **2014**, *50* (61), 8331−8334.
(46) Deshmukh, S. D.; Ellis, R. G.; Sutandar, D. S.; Rokke, D. J.; Agrawal, R. Versatile Colloidal Syntheses of Metal Chalcogenide Nanoparticles from Elemental Precursors Using Amine-Thiol Chemistry. *Chem. Mater.* **2019**, *31*, 9087.
(47) Deshmukh, S. D.; Easterling, L. F.; Manheim, J. M.; LiBretto, N. J.; Weideman, K. G.; Miller, J. T.; Kenttämaa, H. I.; Agrawal, R.

https://doi.org/10.1021/acs.nanolett.3c02620
Nano Lett. 2023, 23, 11430−11437

Analyzing and Tuning the Chalcogen−Amine−Thiol Complexes for Tailoring of Chalcogenide Syntheses. *Inorg. Chem.* **2020**, *59* (12), 8240−8250.
(48) Miller, R. C.; Neilson, J. R.; Prieto, A. L. Amide-Assisted Synthesis of Iron Germanium Sulfide (Fe_2GeS_4) Nanostars: The Effect of $LiN(SiMe_3)_2$ on Precursor Reactivity for Favoring Nanoparticle Nucleation or Growth. *J. Am. Chem. Soc.* **2020**, *142* (15), 7023−7035.
(49) Deka, S.; Genovese, A.; Zhang, Y.; Miszta, K.; Bertoni, G.; Krahne, R.; Giannini, C.; Manna, L. Phosphine-Free Synthesis of p-Type Copper(I) Selenide Nanocrystals in Hot Coordinating Solvents. *J. Am. Chem. Soc.* **2010**, *132* (26), 8912−8914.
(50) Qi, T.; Yang, H.-Q.; Whitfield, D. M.; Yu, K.; Hu, C.-W. Insights into the Mechanistic Role of Diphenylphosphine Selenide, Diphenylphosphine, and Primary Amines in the Formation of CdSe Monomers. *J. Phys. Chem. A* **2016**, *120* (6), 918−931.
(51) Anderson, N. C.; Hendricks, M. P.; Choi, J. J.; Owen, J. S. Ligand Exchange and the Stoichiometry of Metal Chalcogenide Nanocrystals: Spectroscopic Observation of Facile Metal-Carboxylate Displacement and Binding. *J. Am. Chem. Soc.* **2013**, *135* (49), 18536−18548.
(52) Drijvers, E.; De Roo, J.; Martins, J. C.; Infante, I.; Hens, Z. Ligand Displacement Exposes Binding Site Heterogeneity on CdSe Nanocrystal Surfaces. *Chem. Mater.* **2018**, *30* (3), 1178−1186.
(53) Kaseman, D. C.; Jarvi, A. G.; Gan, X. Y.; Saxena, S.; Millstone, J. E. Evolution of Surface Copper(II) Environments in $Cu_{2-x}Se$ Nanoparticles. *Chem. Mater.* **2018**, *30*, 7313−7321.
(54) Liu, M.; Wang, Y. Y.; Liu, Y.; Jiang, F. L. Thermodynamic Implications of the Ligand Exchange with Alkylamines on the Surface of CdSe Quantum Dots: The Importance of Ligand-Ligand Interactions. *J. Phys. Chem. C* **2020**, *124* (8), 4613−4625.
(55) Jain, A.; Ong, S. P.; Hautier, G.; Chen, W.; Richards, W. D.; Dacek, S.; Cholia, S.; Gunter, D.; Skinner, D.; Ceder, G.; Persson, K. A. Commentary: The Materials Project: A Materials Genome Approach to Accelerating Materials Innovation. *APL Mater.* **2013**, *1* (1), No. 011002.
(56) Sheldon, R. A. The: E Factor 25 Years on: The Rise of Green Chemistry and Sustainability. *Green Chem.* **2017**, *19* (1), 18−43.
(57) Platt, J. R. Strong Inference. *Science* **1964**, *146*, 347−353.
(58) Chamberlin, T. C. The Method of Multiple Working Hypotheses. *Science* **1965**, *148* (3671), 754−759.
(59) Scott, S. L. The Burden of Disproof. *ACS Catal.* **2019**, *9* (5), 4706−4708.
(60) Whitehead, C. B.; Finke, R. G. Particle Formation Mechanisms Supported by in Situ Synchrotron XAFS and SAXS Studies: A Review of Metal, Metal-Oxide, Semiconductor and Selected Other Nanoparticle Formation Reactions. *Mater. Adv.* **2021**, *2* (20), 6532−6568.
(61) Olofsson, O.; Holmlund, L.; Ingri, N.; Tricker, M. J.; Svensson, S. The Crystal Structure of Cu_3P. *Acta Chem. Scand.* **1972**, *26*, 2777−2787.
(62) De Trizio, L.; Gaspari, R.; Bertoni, G.; Kriegel, I.; Moretti, L.; Scotognella, F.; Maserati, L.; Zhang, Y.; Messina, G. C.; Prato, M.; Marras, S.; Cavalli, A.; Manna, L. $Cu_{3-x}P$ Nanocrystals as a Material Platform for near-Infrared Plasmonics and Cation Exchange Reactions. *Chem. Mater.* **2015**, *27* (3), 1120−1128.
(63) Tappan, B. A.; Chen, K.; Lu, H.; Sharada, S. M.; Brutchey, R. L. Synthesis and Electrocatalytic HER Studies of Carbene-Ligated $Cu_{3-x}P$ Nanocrystals. *ACS Appl. Mater. Interfaces* **2020**, *12* (14), 16394−16401.
(64) Rachkov, A. G.; Schimpf, A. M. Colloidal Synthesis of Tunable Copper Phosphide Nanocrystals. *Chem. Mater.* **2021**, *33* (4), 1394−1406.
(65) Scardi, P. Diffraction Line Profiles in the Rietveld Method. *Cryst. Growth Des.* **2020**, *20* (10), 6903−6916.
(66) Saunders, A. P. The Allotropic Forms of Selenium. *J. Phys. Chem.* **1900**, *4* (6), 423−513.
(67) Das Gupta, K.; Das, S. R.; Ray, B. B. A Study of Allotropes of Selenium by the X-Ray Diffraction Method. *Indian J. Phys.* **1941**, *11*, 389−399.
(68) Murphy, K. E.; Altman, M. B.; Wunderlich, B. The Monoclinic-to-Trigonal Transformation in Selenium. *J. Appl. Phys.* **1977**, *48* (10), 4122−4131.
(69) Gerlach, E.; Grosse, P. *The Physics of Selenium and Tellerium*, 1st ed.; Springer Berlin, Heidelberg: Koenigstein, 1979.
(70) Wunderlich, B.; Shu, H.-C. The Crystallization and Melting of Selenium. *J. Cryst. Growth* **1980**, *48* (2), 227−239.
(71) Corb, B. W.; Wei, W. D.; Averbach, B. L. Atomic Models of Amorphous Selenium. *J. Non-Cryst. Solids* **1982**, *53* (1−2), 29−42.
(72) Jóvári, P.; Delaplane, R. G.; Pusztai, L. Structural Models of Amorphous Selenium. *Phys. Rev. B* **2003**, *67* (17), No. 172201.
(73) Bisht, N.; Phalswal, P.; Khanna, P. K. Selenium Nanoparticles: A Review on Synthesis and Biomedical Applications. *Mater. Adv.* **2022**, *3* (3), 1415−1431.
(74) Ruiz-Fresneda, M. A.; Staicu, L. C.; Lazuén-López, G.; Merroun, M. L. Allotropy of Selenium Nanoparticles: Colourful Transition, Synthesis, and Biotechnological Applications. *Microb. Biotechnol.* **2023**, *16* (5), 877−892.
(75) Chu, J. Y. C.; Marsh, D. G.; Guenther, W. H. H. Photochemistry of Organochalcogen Compounds. I. Photolysis of Benzyl Diselenide. *J. Am. Chem. Soc.* **1975**, *97* (17), 4905−4908.
(76) Sperry, B. M.; Luscombe, C. K. Ligand Pyrolysis during Air-Free Inorganic Nanocrystal Synthesis. *Chem. Mater.* **2021**, *33* (1), 136−145.
(77) Calcabrini, M.; Van den Eynden, D.; Ribot, S. S.; Pokratath, R.; Llorca, J.; De Roo, J.; Ibáñez, M. Ligand Conversion in Nanocrystal Synthesis: The Oxidation of Alkylamines to Fatty Acids by Nitrate. *JACS Au* **2021**, *1* (11), 1898−1903.
(78) Huang, Y.; Kong, F.; Pei, F.; Wang, L.; Cui, X.; Shi, J. Modulating the Electronic Structure of Hollow Cu/Cu_3P Heteronanoparticles to Boost the Oxygen Reduction Performance in Long-lasting Zn-air Battery. *EcoMat* **2023**, *5* (5), No. e12335.
(79) Wei, S.; Qi, K.; Jin, Z.; Cao, J.; Zheng, W.; Chen, H.; Cui, X. One-Step Synthesis of a Self-Supported Copper Phosphide Nanobush for Overall Water Splitting. *ACS Omega* **2016**, *1* (6), 1367−1373.
(80) Zhou, X.; Zhou, X.; Liu, L.; Chen, H.; Hu, X.; Qian, J.; Huang, D.; Zhang, B.; Tang, J. Self-Supported Cu_3P Nanowire Electrode as an Efficient Electrocatalyst for the Oxygen Evolution Reaction. *RSC Adv.* **2021**, *11* (54), 34137−34143.
(81) Yin, Y.; Zhang, Y.; Liu, N.; Sun, B.; Zhang, N. Biomass-Derived P/N-Co-Doped Carbon Nanosheets Encapsulate Cu_3P Nanoparticles as High-Performance Anode Materials for Sodium−Ion Batteries. *Front. Chem.* **2020**, *8*, No. 316.
(82) Dang, R.; Xu, X.; Xie, M.; Liu, J. Synthesis of Self-Supported Cu/Cu_3P Nanoarrays as an Efficient Electrocatalyst for the Hydrogen Evolution Reaction. *Catalysts* **2022**, *12* (7), 762.
(83) Lin, J.; Zeng, C.; Lin, X.; Xu, C.; Su, C. CNT-Assembled Octahedron Carbon-Encapsulated Cu_3P/Cu Heterostructure by In Situ MOF-Derived Engineering for Superior Lithium Storage: Investigations by Experimental Implementation and First-Principles Calculation. *Adv. Sci.* **2020**, *7* (14), No. 2000736.
(84) Zhao, W.; Zhou, H.; Lu, K.; Li, Y.; Shi, W.; Ma, X. Electronic/Ionic Engineering Inspired Formation of Carbon-Encapsulated Cu_3PSe_4/Cu_2Se Heterostructured Hollow Nanosphere for Trace Level Neurochemical Monitoring. *Appl. Surf. Sci.* **2023**, *613*, No. 156142.
(85) Kumar, D.; Gohil, S.; Gokhale, M.; Chalke, B.; Ghosh, S. Revisiting the Problem of Crystallisation and Melting of Selenium. *J. Phys.: Condens. Matter* **2021**, *33* (29), No. 295402.
(86) Lu, J.; Xie, Y.; Xu, F.; Zhu, L. Study of the Dissolution Behavior of Selenium and Tellurium in Different Solvents—a Novel Route to Se, Te Tubular Bulk Single Crystals. *J. Mater. Chem.* **2002**, *12* (9), 2755−2761.
(87) Iida, Y.; Yamaguchi, T.; Tanaka, T.; Nakayama, S. Solubility of Selenium at High Ionic Strength under Anoxic Conditions. *J. Nucl. Sci. Technol.* **2010**, *47* (5), 431−438.
(88) Webber, D. H.; Buckley, J. J.; Antunez, P. D.; Brutchey, R. L. Facile Dissolution of Selenium and Tellurium in a Thiol−Amine

https://doi.org/10.1021/acs.nanolett.3c02620
Nano Lett. 2023, 23, 11430−11437

Solvent Mixture under Ambient Conditions. *Chem. Sci.* **2014**, *5* (6), 2498−2502.
(89) Grunwald, H. P. Crystalline Growth of Monoclinic Selenium. *Mater. Res. Bull.* **1972**, *7* (10), 1093−1100.
(90) Chung, C.-H.; Li, S.-H.; Lei, B.; Yang, W.; Hou, W. W.; Bob, B.; Yang, Y. Identification of the Molecular Precursors for Hydrazine Solution Processed $CuIn(Se,S)_2$ Films and Their Interactions. *Chem. Mater.* **2011**, *23* (4), 964−969.
(91) Wuyts, H.; Stewart, A. L. Une Préparation de l'hydrogène Sélénié. *Bulletin de la Sociéte chimique de Belgique* **1909**, *23*, 9−11.
(92) Green, C.; Bradt, W. E. The Preparation of Hydrogen Selenide by the Interaction of Selenium and Hydrocarbons. *Proc. Indiana Acad. Sci.* **1933**, *43*, 116−118.
(93) Shen, H.; Niu, J.; Wang, H.; Li, L. S. One-Pot Synthesis of High Quality CdE (E = Te, Te_xSe_{1-x}, Se) Nanocrystals without Using Pyrophoric Reagents. *Mater. Chem. Phys.* **2012**, *135* (2−3), 1122−1127.
(94) Olin, A.; Nolang, B.; Osadchii, E.; Ohman, L.-O.; Rosen, E. *Chemical Thermodynamics of Selenium*, Vol. *7*; Elsevier, 2004.

https://doi.org/10.1021/acs.nanolett.3c02620
Nano Lett. 2023, 23, 11430−11437